LIMNOLOGY
and
OCEANOGRAPHY

ASLO

Limnol. Oceanogr. 61, 2016, S150–S164
© 2016 Association for the Sciences of Limnology and Oceanography
doi: 10.1002/lno.10311

High methane emissions from thermokarst lakes in subarctic peatlands

Alex Matveev,[1,2] Isabelle Laurion,[1,3] Bethany N. Deshpande,[1,2] Najat Bhiry,[1,4] Warwick F. Vincent*[1,2]
[1]Centre d'études nordiques - Centre for Northern Studies (CEN), Québec City, Québec, Canada
[2]Département de biologie & Takuvik, Université Laval, Québec City, Québec, Canada
[3]Centre Eau Terre Environnement, INRS, Québec City, Québec, Canada
[4]Département de géographie, Université Laval, Québec City, Québec, Canada

Abstract

The thawing and subsidence of frozen peat mounds (palsas) in permafrost landscapes results in the formation of organic-rich thermokarst lakes. We examined the effects of palsa degradation on CH_4 and CO_2 emissions by comparing thermokarst lakes at two peatland locations in subarctic Québec, Canada: in the northern discontinuous permafrost region, and in southern sporadic permafrost where palsas are more rapidly degrading. The lakes were shallow (< 3 m) but stratified at both sites, and most had anoxic bottom waters. The surface waters at both sites were supersaturated in CH_4 and CO_2, and to a greater extent in the southern lakes, where the surface CH_4 concentrations were up to 3 orders of magnitude above air equilibrium. Concentrations of CH_4 and CO_2 increased by orders of magnitude with depth in the southern lakes, however these gradients were less marked or absent in the North. Strong CH_4 and CO_2 emissions were associated with gas ebullition, but these were greatly exceeded by diffusive fluxes, in contrast to thermokarst lakes studied elsewhere. Also unusual relative to other studies to date, the surface concentrations of both gases increased as a linear function of water column depth, with highest values over the central, deepest portion of the lakes. Radiocarbon dating of ebullition gas samples showed that the CH_4 had ^{14}C-ages from 760 yr to 2005 yr before present, while the CO_2 was consistently younger. Peatland thermokarst lakes may be an increasingly important source of greenhouse gases as the southern permafrost limit continues to shift northwards.

Global levels of atmospheric methane (CH_4) continue to rise, with values close to 2 ppm observed locally in the Arctic (NOAA 2014). The origins of this CH_4 are uncertain, and one source of uncertainty is the net flux to the atmosphere from thermokarst lakes and ponds (Negandhi et al. 2013; Tan et al. 2015). These waterbodies are formed by the thawing and collapse of ice-rich permafrost (Hopkins 1949), and they have been recognized as sites of intense biogeochemical activity in northern landscapes (Vincent et al. 2013, and references therein). Permafrost soils have the potential to release 68 to 508 Pg of carbon by 2100, depending on different response scenarios (MacDougall et al. 2012); however the current estimates of greenhouse gas (GHG) emissions from thermokarst lakes range from major (Schuur et al. 2013) to insignificant (Gao et al. 2013). This large variability in estimates is in part related to the diversity of thermokarst lake types, and the sparseness of observations across the circumpolar North.

Much of the emphasis to date on measuring gas fluxes from thermokarst lakes has focused on water bodies that are located on yedoma, wind-blown surface deposits that cover vast areas of Siberia and Alaska. Yedoma permafrost soils contain 1–5% organic carbon (Tarnocai et al. 2009), and the thermokarst lakes in these landscapes have elevated rates of CH_4 release, dominated by ebullition. For example, in a comparison of 40 Alaskan lakes along a north-south transect, the CH_4 emissions were sixfold higher than from non-yedoma lakes, the latter including waters unaffected by permafrost; ebullition accounted for 86% and 65% of the annual CH_4 emissions from yedoma and non-yedoma lakes, respectively (Sepulveda-Jauregui et al. 2015). In general, however, there is a sparseness of information about the biogeochemistry of non-yedoma thermokarst lakes, despite an estimated storage of 75% of the global carbon permafrost pool in non-yedoma permafrost (Vonk et al. 2015).

Non-yedoma thermokarst lakes include water bodies associated with the collapse of palsas, ice-rich permafrost mounds and plateaus that are found in northern peatlands,

*Correspondence: warwick.vincent@fsg.ulaval.ca

Additional Supporting Information may be found in the online version of this article.

Special Issue: Methane Emissions from Oceans, Wetlands, and Freshwater Habitats: New Perspectives and Feedbacks on Climate.
Edited by: Kimberly Wickland and Leila Hamdan.

particularly in subarctic regions of discontinuous permafrost (e.g., Karlsson et al. 2010; Saemundsson et al. 2012). These mounds form during periods of climatic cooling and permafrost aggradation, and they rise up to 10 m above the initial ground level as a result of interstitial water and groundwater that is aspirated towards growing ice lenses in fine sediments at the base of the mound ("cryosuction"); this uplifts the overlying frozen peat, which in turn reduces snow accumulation and favors the cooling, freezing and ongoing mound development (An and Allard 1995). These periglacial features are sensitive to subsequent increases in temperature and precipitation, and their thawing and collapse result in thermokarst basins that fill with water, derived in part from the melting ice (Luoto and Seppälä 2003). Palsas contain a large organic carbon pool, with concentrations around 50% dry weight (Krüger et al. 2014). This is an order of magnitude higher than yedoma soils (Tarnocai et al. 2009), and although the lability of this moss-derived material is uncertain, observations in northern Norway point to degrading palsa soils as sites of abundant methanogens and high rates of methanogenesis, particularly during the thermokarst pond stage, prior to eventual infilling by sediment and plants (Liebner et al. 2015).

Our primary objective in the present study was to quantify the CH_4 and CO_2 emissions from thermokarst lakes formed by subsiding palsas in subarctic peatlands. We undertook this research in northern Québec (Nunavik), where mean annual air temperatures have increased over the last three decades, and where permafrost thawing and degradation are proceeding rapidly (Bhiry et al. 2011; Bouchard et al. 2015). We aimed to determine the age of the source carbon of these emissions for comparison with the stratigraphic history of these sites, and to evaluate the relative importance of gas fluxes to the atmosphere via ebullition and diffusion. We hypothesized that climate-induced thawing and expansion of palsa-associated thermokarst lakes would mobilize ancient carbon reserves and would stimulate CH_4 and CO_2 emissions as a result of the aquatic microbial degradation of these materials. To address this hypothesis, we measured the concentrations, surface fluxes and ^{14}C age of CH_4 and CO_2 along with profiles of limnological variables in thermokarst lakes at two contrasting peatland sites: in a valley of rapidly degrading palsas near the southern permafrost limit, and in a colder palsa valley located further to the North where permafrost degradation is less advanced. We also examined the questions of how gas emissions in these waters vary as a function of water depth and within a 24-h period of repeated sampling.

Methods and materials

Study sites

The sampled lakes and ponds (hereafter referred to as thermokarst lakes) lie in two peatland valleys, at southern and northern locations in subarctic Québec, Canada (Fig. 1; Supporting Information Table S1). Sampling took place during mid- to late summer (July–August) over the course of three field seasons (2012, 2013, 2014). The vegetation in both valleys includes mixed shrubs and semi-aquatic plants, notably *Carex aquatilis, Carex rariflora*, and *Eriophorum angustifolium*. Both valleys also contain small stands and isolated individuals of black spruce (*Picea mariana*).

The southern thermokarst lakes are in the valley of the Sasapimakwananisikw River (hereafter SAS valley), 8 km southwest of the village of Whapmagoostui-Kuujjuarapik. Sampling in the SAS valley was at two locations: thermokarst lakes formed alongside palsas north of the river at 55°13′N, 77°41′W (SAS2 lakes), and similar palsa-associated lakes located south of the river at 55°13′N, 77°42′W (SAS1 lakes). The SAS lakes are located in the sporadic permafrost zone, near the southern limit of subarctic permafrost that underlies $< 2\%$ of the land surface, and now mostly present in the remaining palsa mounds. Stratigraphic and macrofossil analyses of this valley (Arlen-Pouliot and Bhiry 2005; Fillion et al. 2014) have shown that the organic soil deposits date back to 5800 yr BP and are underlain by marine clays derived from the Tyrell Sea, which flooded the area immediately after ice retreat around 8000 yr BP. The soil stratigraphy shows periods of marsh, bog, and fen development with the most recent moss peatland bog forming between approximately 2100 yr BP to 400 yr BP. Permafrost development took place during the Little Ice Age (LIA), from 400 yr BP to 200 yr BP, with the formation of palsas that likely fused to form an extensive frozen peatland plateau. The valley currently has more than 100 palsas, mostly 3–5 m in height. Permafrost thawing in this region dates from the end of the LIA onwards (ca. 150 yr BP) and resulted in the production of thermokarst lakes and ponds. Some of these have now filled in completely, while others are newly formed or are continuing to expand.

The northern thermokarst lakes are located 280 km north of the SAS valley, 136 km north of the village of Umiujaq and 10 km south of the treeline, in the palsa-rich floodplain of the Boniface River at 57°45′N, 77°20′W (BON lakes). This site is in the subarctic discontinuous permafrost zone, where the permafrost extends over more than 50% of the landscape (Allard and Seguin 1987). Stratigraphic and macrofossil analyses at this site (Bhiry et al. 2007) have shown that peat formed over marine silt from around 6800 yr BP onwards, with subsequent periods of accumulation and decomposition. In contrast to the SAS site where the palsas formed only during the LIA, three phases of permafrost aggradation and palsa development have been identified at BON: 3200 yr, 2000 yr, and 400 yr BP, but with most of the palsas formed during the LIA. These are elongate mounds mostly around 6.5 m high, separated by linear moist depressions including thermokarst lakes. The lakes likely began to form subsequent to the LIA, with expansion over the 20th century.

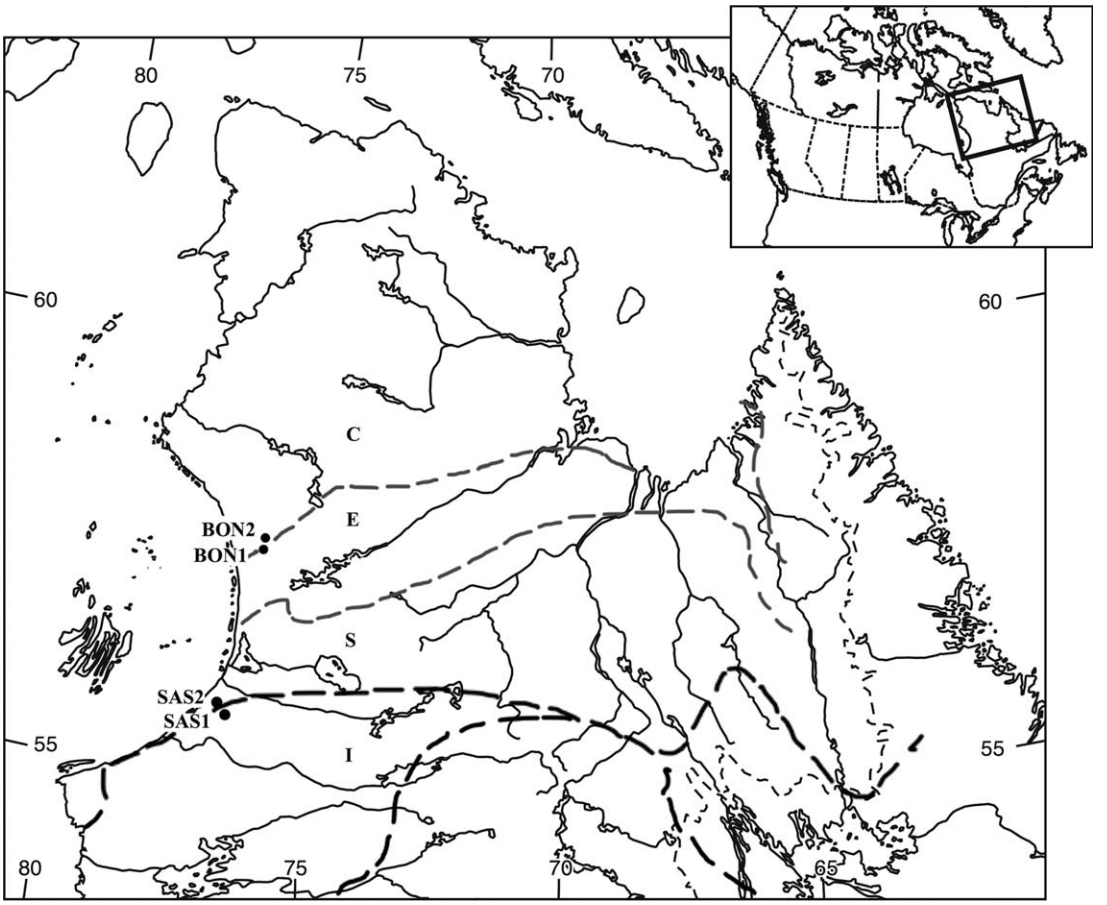

Fig. 1. Study sites and permafrost distribution in subarctic Québec (Nunavik), Canada. BON1 and 2: the northern palsa lake sites in the vicinity of the Boniface River. SAS1 and 2: the southern palsa lake sites in the Sasapimakwananisikw River valley. C, E, S, and I denote zones of continuous (**C**, 90–100% of land area underlain by permafrost), discontinuous extended (**E**, 50–90% frozen), discontinuous sporadic (**S**, 10–50%), and isolated patches (**I**, 0–10%) of permafrost in the region of study (data from Allard and Seguin 1987).

A comparison of aerial photographs of this region showed that the total surface area of palsas decreased by 23% between 1957 and 2001, while the area of thermokarst lakes and ponds increased by 76%; these changes were much less extensive, however, than at southern, warmer sites in subarctic Québec (Vallée and Payette 2007), and palsa subsidence appears to be proceeding more slowly than in the SAS valley at this northern cooler site.

Air and ground temperatures

Air and ground temperatures were measured at minute intervals with YSI 44033 thermistors (Yellow Springs Instruments, Yellow Springs, Ohio, U.S.A.; accuracy $\pm < 0.1$°C in the observed range; response time 0.12 s to 10 s), and the averages were recorded each hour in a Campbell CR10 data logger (Campbell Scientific, Edmonton, AB, Canada; accuracy $\pm$ 0.02%). The air temperature probes were housed in radiation screens (RM Young 6 plate radiation shield; Campbell Scientific, Edmonton, Alberta, Canada) and positioned 2 m above the ground. The ground temperatures were measured in boreholes drilled into a palsa mound at SAS2 to a depth of 5 m, and in a hole dug into gravel soils to a depth of 1.0 m at BON (Allard et al. 2015).

Limnological profiling

Vertical profiles of temperature ($\pm$ 0.15°C), conductivity ($\pm$ 0.001 mS cm^{-1}), oxygen ($\pm$ 0.2 mg L^{-1}), and pH ($\pm$ 0.2 units) were recorded using a YSI 6000 profiler (Yellow Springs Instruments, Yellow Springs, Ohio, U.S.A.) with all sensors calibrated and verified according to manufacturer specifications. Vertical profiles of photosynthetically available radiation (PAR; $\pm$ 1%) were obtained with a LI-192 Underwater PAR Quantum Sensor (LI-COR Biosciences, Lincoln, Nebraska, U.S.A.).

Near-surface lake water samples were collected in 125 mL borosilicate amber glass bottles (Wheaton, Millville, New Jersey, U.S.A.) for total and soluble reactive phosphorus (TP and SRP) and total nitrogen (TN), and analyzed with a Lachat Autoanalyzer according to the methods of Stainton et al. (1977). The detection limits were 0.001 mg TP L^{-1}, 0.5

μg SRP L^{-1}; and 0.02 mg TN L^{-1}. Dissolved organic carbon (DOC) was analyzed in water samples that were filtered through pre-rinsed 0.2-μm cellulose acetate filters (4°C) and measured by high temperature catalytic combustion in a Total Organic Carbon analyzer (Shimadzu VCPH, TOC-5000A) calibrated with potassium biphthalate (detection limit of 0.05 mg DOC L^{-1}). Phytoplankton biomass was estimated from the chlorophyll *a* concentration (Chl-*a*) quantified by high performance liquid chromatography using the methods as in Bonilla et al. (2005).

Gas concentrations and fluxes

Water for gas concentrations was sampled with a thin-layer sampler based on the design shown in Fig. 2.4 of Golterman and Clymo (1971). This was composed of two 140-mm diameter circular thermoplastic plates that were set 63.5 mm apart. The upper plate was drilled with a 6.4 mm diameter central hole, which was fitted with a tube that extended to a peristaltic pump onboard the boat. The pump was adjusted to a constant speed to allow laminar flow (Reynolds number = 5.6×10^{-5}) and the sampler was lowered through the water column to collect samples at 0.1 m depth intervals. The water was pumped into 2-liter LDPE bottles that were overfilled three times. Immediately after collection (on site), 20 mL of lakewater was replaced by ambient air using a syringe connected to the bottom of bottle to create a headspace; the bottle was then vigorously shaken for 3 min to extract the dissolved gases, and the headspace was subsampled (Hesslein et al. 1990). Ambient air samples were also taken directly in situ. All samples (10 mL) were stored in 5.9 mL Labco Exetainer vials (Labco Limited, UK) that were sealed with butyl rubber septa. These had been previously flushed with helium and evacuated, and the vials were kept at cool temperature until laboratory analysis.

Concentrations of CH_4 and CO_2 in the samples were determined by gas chromatography with flame ionization detection (Varian 3800, COMBI PAL head space injection system, CP-Poraplot Q 25m with flame ionization detector). The diffusive flux (F) at the air–water interface was calculated as Fickian diffusion corrected for low solubility gases (Vachon et al. 2010):

$$F = k \cdot K_H \cdot \Delta P \quad (1)$$

where k is the gas transfer velocity of either CO_2 or CH_4, K_H is the Henry's constant, and ΔP is the air–water gradient of the partial gas pressure. The k values were calculated using Cole and Caraco (1998) parameterization, and the Schmidt numbers were computed according to the algorithm given in Crusius and Wanninkhof (2003). A correction for near–surface wind mixing was made using the wind model of MacIntyre et al. (2010) adjusted for the energy loss by surface cooling. The horizontal component of wind speed was measured at 2 m above the lake surface with a portable Kestrel weather probe (Kestrel 4500, Nielsen-Kellerman Co., Boothwyn, PA; range 0.4–60.0 m s^{-1}, resolution 0.1, accuracy ± 3% of least significant digit) and averaged over 10 min. These values were then corrected to provide wind speed at 10 m; these extrapolations were made as in Vachon et al. (2010) assuming a logarithmic wind profile.

CH_4, CO_2 and O_2 concentrations were also measured in the water column using an automated continuous GHG monitoring system. This instrument measured gas concentrations with three independent sensors in a gas stream equilibrated with the source water; further details are provided in Bastien et al. (2009) and Laurion et al. (2010).

Gas emissions by ebullition were measured using opaque submerged gas traps. They consisted of a gas–tight inversed funnel with a 0.5 m^2 opening at the bottom, and a 140 mL plastic syringe (Kendall Monoject^{TM} piston syringe) mounted on the top and closed with a one-way luer-lock valve. Each trap was installed with the opening submerged at a depth of 0.5 m, for 12 h to 36 h (depending on ebullition rates). Two to five traps were deployed per lake on each sampling date, along transects from inshore to offshore sites. At the end of each deployment, the accumulated gas was transferred to 5.9 mL Labco Exetainer vials as above for subsequent analysis.

Radiocarbon dating

A gas volume of 100 mL was collected from some of the gas traps, for ^{14}C-dating of CO_2 and CH_4. These samples were transferred to pre-vacuumed 50 mL serum bottles (Wheaton, U.S.A.) closed with a thick butyl rubber stopper (Chemglass Life Science, U.S.A.) and were subsequently analyzed by accelerator mass spectrometry (AMS) at the Keck Carbon Cycle AMS Facility of the University of California, Irvine, California, U.S.A., as in Bouchard et al. (2015). Firstly, CH_4 and CO_2 were separated by a continuous flow line consisting of purification and combustion traps: CO_2 was frozen in liquid nitrogen, then carbon monoxide (CO) was oxidized to CO_2 in a 300°C CuO furnace and frozen in a second liquid nitrogen trap, and finally noncondensable CH_4 was oxidized to CO_2 in a CuO furnace at 975°C (Lindberg/Blue M Tube Furnace, Thermo Scientific). The resulting CO_2 and H_2O from CH_4 combustion were further separated cryogenically on the vacuum line, and the purified CO_2 was graphitized using the sealed tube zinc reduction method. This laboratory reports a day-to-day analysis relative error of 2.5‰ to 3.1‰ based on secondary standards, and including extraction, graphitization and AMS measurement. A sediment core was also obtained from Lake SAS1B at the deepest point in the lake with a mini-Glew gravity corer, and the black, flocculent organic over layer (top 0–3 cm) along with three cohesive, deeper layers of organic sediment (3–6, 6–10, and 10–12 cm) were dated. These were also analyzed at the Keck Carbon Cycle AMS Facility. The ^{14}C results were expressed as fractions of the modern standard, $\Delta^{14}C$, and conventional

radiocarbon age following Stuiver and Polach (1977). All results were corrected for isotopic fractionation.

Results

Air and ground temperatures

The mean annual air temperature measured at the southern SAS site (−3.42°C) was ca. 2.4°C higher than at the northern BON site (Fig. 2), and the number of thawing degree-days was 26% higher (1437 vs. 1144°C-days). The ground temperature thermistors showed that both sites exhibited large seasonal temperature variations (Fig. 2a), and that the palsa permafrost core remained at temperatures below freezing even at the southern (SAS) site (Fig. 2b). The palsa at SAS2 had an active layer that extended down to 0.6 m depth (Fig. 3). Permafrost temperatures varied seasonally below that depth, down to 3.5 m, where the changes were minimal throughout the year (Fig. 3, inset), with the zero annual amplitude depth at 3.55 m. The permafrost temperature at that site was only slightly below freezing (−0.48°C).

Limnological profiling

All of the palsa lakes were thermally stratified on all dates of observation. However, the southern (SAS) lakes showed stronger and more stable stratification, especially towards the end of the open water season. This tendency corresponded to the greater light attenuation in the SAS lakes, with 1% irradiance found around 0.25 m depth vs. almost 1 m in the northern (BON) palsa lakes (Figs. 4a,b,c, 5a,b,c).

Lakes at both northern and southern locations demonstrated a decrease in pH with depth. The BON lakes (Fig. 4d,e,f) ranged from close to neutral pH = 6.8 at the surface (Fig. 4d) to acidic pH < 5.0 at the bottom (Fig. 4f). The southern SAS lakes had more acidic waters throughout the entire water column (Fig. 5d–f), with a maximum value of pH = 6.2 at the surface of the lake SAS2A and a minimum of pH = 4.5 just below the oxycline in that lake (Fig. 5e). There were also large differences in specific conductivity particularly at the bottom of these lakes. While of similar magnitude at the surface (BON = 2.9 ± 0.7 mS m^{-1}; SAS = 4.6 ± 0.3 mS m^{-1}), specific conductivity increased sharply with depth in the SAS lakes (up to 21 mS m^{-1} in SAS2A lake, Fig. 5e), but stayed around the same order of magnitude (around 1.2 mS m^{-1}) throughout the entire water column towards the bottom of BON lakes (Fig. 4d–f).

Surface waters at both locations were undersaturated in O_2. Despite their shallow depths, all palsa lakes exhibited oxygen stratification during the entire period of observation, with strongest stratification in August in the southern SAS lakes, where hypoxic conditions prevailed from 0.4 m down to the bottom of the water column (Fig. 5g,h,k). Most of the lakes had anoxic bottom waters; an exception was lake BON2A where there was an unusual increase to 5 mg O_2 L^{-1}

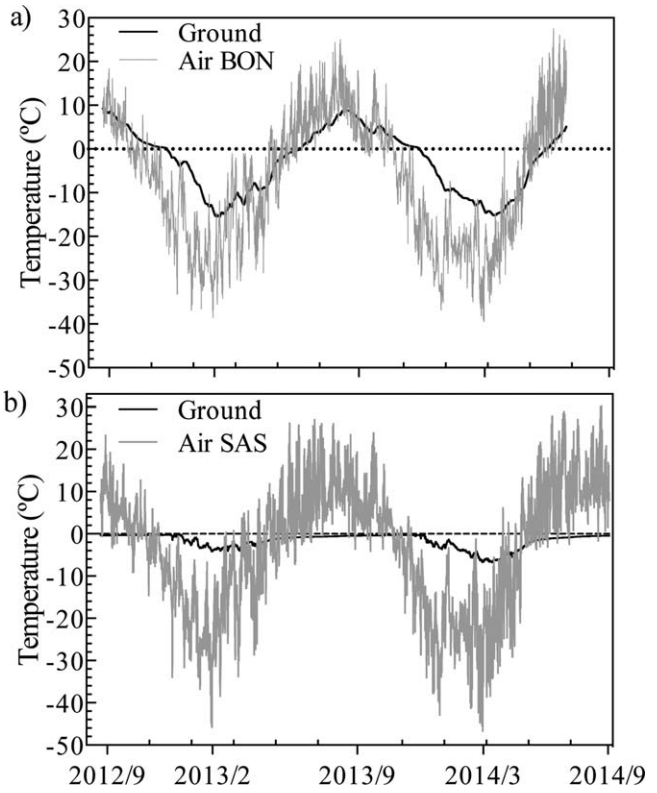

Fig. 2. Air and ground temperatures at northern BON **(a)** and southern SAS **(b)** study sites during the study period. The ground temperature records are from thermistors installed at a depth of 1 m near BON palsas or inside a palsa mound at SAS.

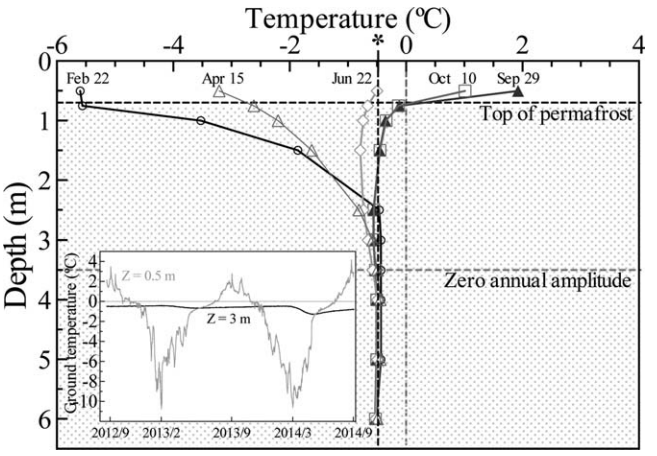

Fig. 3. Ground temperature profiles and annual variations in the palsa at site SAS2A. The vertical dashed line marked by the asterisk (*) denotes the palsa permafrost core temperature of −0.48°C. The dashed horizontal lines mark the depth of the permafrost table (0.65 m) and the zero annual amplitude depth (3.55 m). Days of the months label the corresponding temperature profiles in 2013. Inset: Ground temperature at 0.5 m and 3 m depth at site SAS2A in 2012–2014.

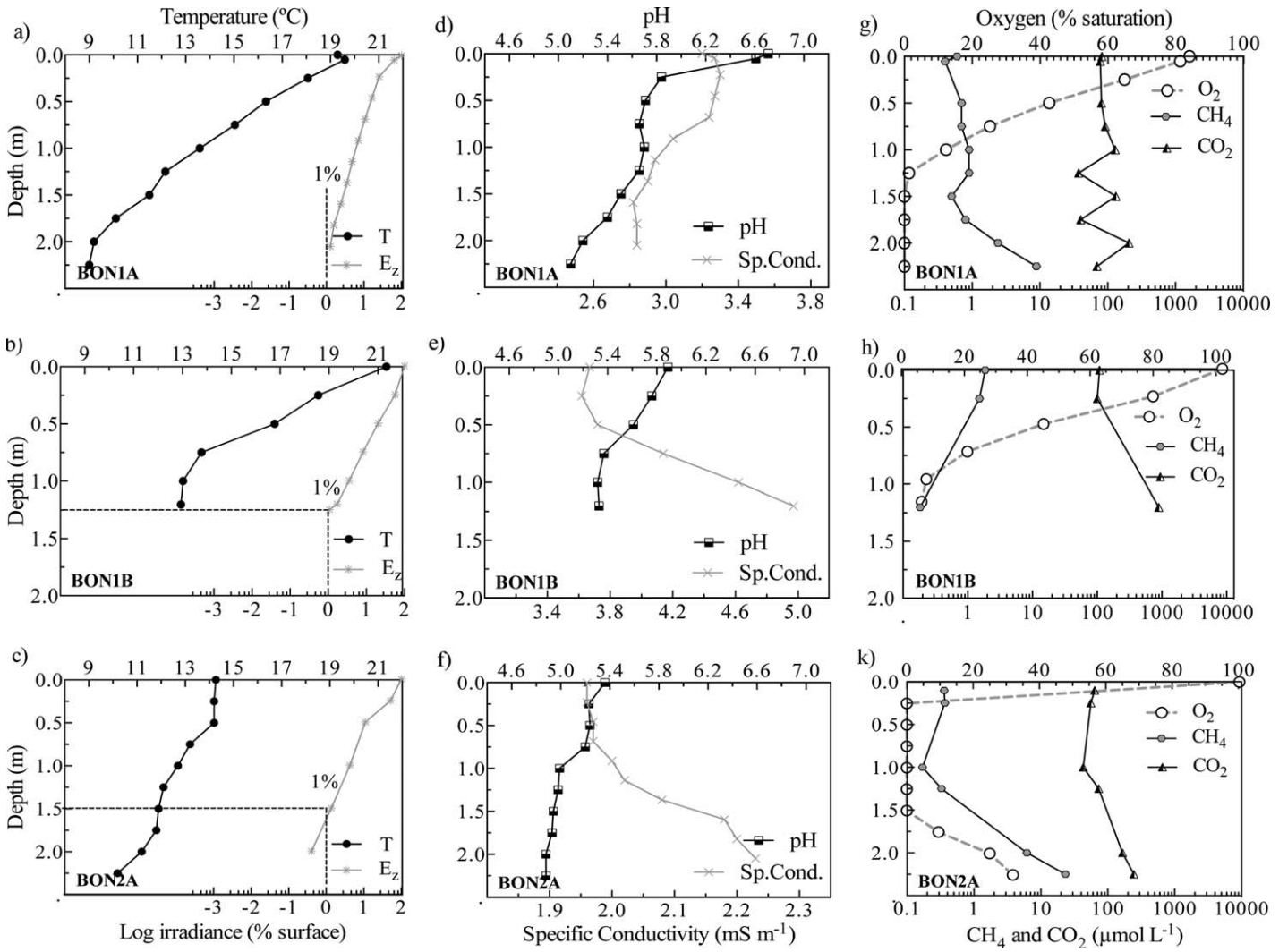

Fig. 4. Limnological profiles in northern palsa lakes BON1A (top three panels), BON1B (middle three panels), and BON2A (lower three panels). Panels **a**, **b**, and **c** show vertical profiles of downwelling PAR irradiance E_z (as % of surface value) and water temperature T (°C), panels **d**, **e**, and **f** show the changes in pH and specific conductivity (Sp.Cond.) down the water column, and panels **g**, **h**, and **k** present vertical profiles of dissolved gas concentrations: dissolved oxygen (as % saturation), CH_4 and CO_2 (in μmol L^{-1}).

near the bottom (Fig. 4k), possibly related to groundwater inflow.

CH_4 and CO_2 concentrations and fluxes

All of the palsa lakes were organic-rich (> 5 mg DOC L^{-1}) and had high concentrations of CH_4 and CO_2 (Table 1). The surface concentrations of both gases were at least one order of magnitude greater in the southern sites compared to those of northern sites in the less degraded palsa fields, and both exceeded the air equilibrium values on average by one order of magnitude for CO_2 and by three orders of magnitude for CH_4 (Table 2).

The gas concentrations increased with depth, especially in the southern SAS lakes (Tables 1, 2). The vertical gradients of CH_4 and CO_2 concentrations down the water column were steeper in the southern palsa lakes than in the northern lakes (Figs. 4, 5). Gas concentrations increased towards the bottom of SAS lakes by 3 (CH_4) and 2 (CO_2) orders of magnitude respectively (Fig. 5g,h,k). In two of the northern lakes, BON1A and BON2A, CH_4 concentrations increased in deeper waters ($Z > 2$ m) by ca. 2 orders of magnitude in the anoxic hypolimnion (Fig. 4g,k), while the shallow (1.3 m) lake BON1B exhibited a small decrease in CH_4 concentrations with depth (Fig. 4h). CO_2 concentrations varied little throughout the water column of lake BON1A (Fig. 4g), but increased by an order of magnitude in lakes BON1B (Fig. 4h) and BON2A (Fig. 4k).

Such gradients at the air-water interface generated large diffusive fluxes of both CH_4 and CO_2 (Table 3). Large ebullition fluxes were also recorded in the lakes, but the diffusive

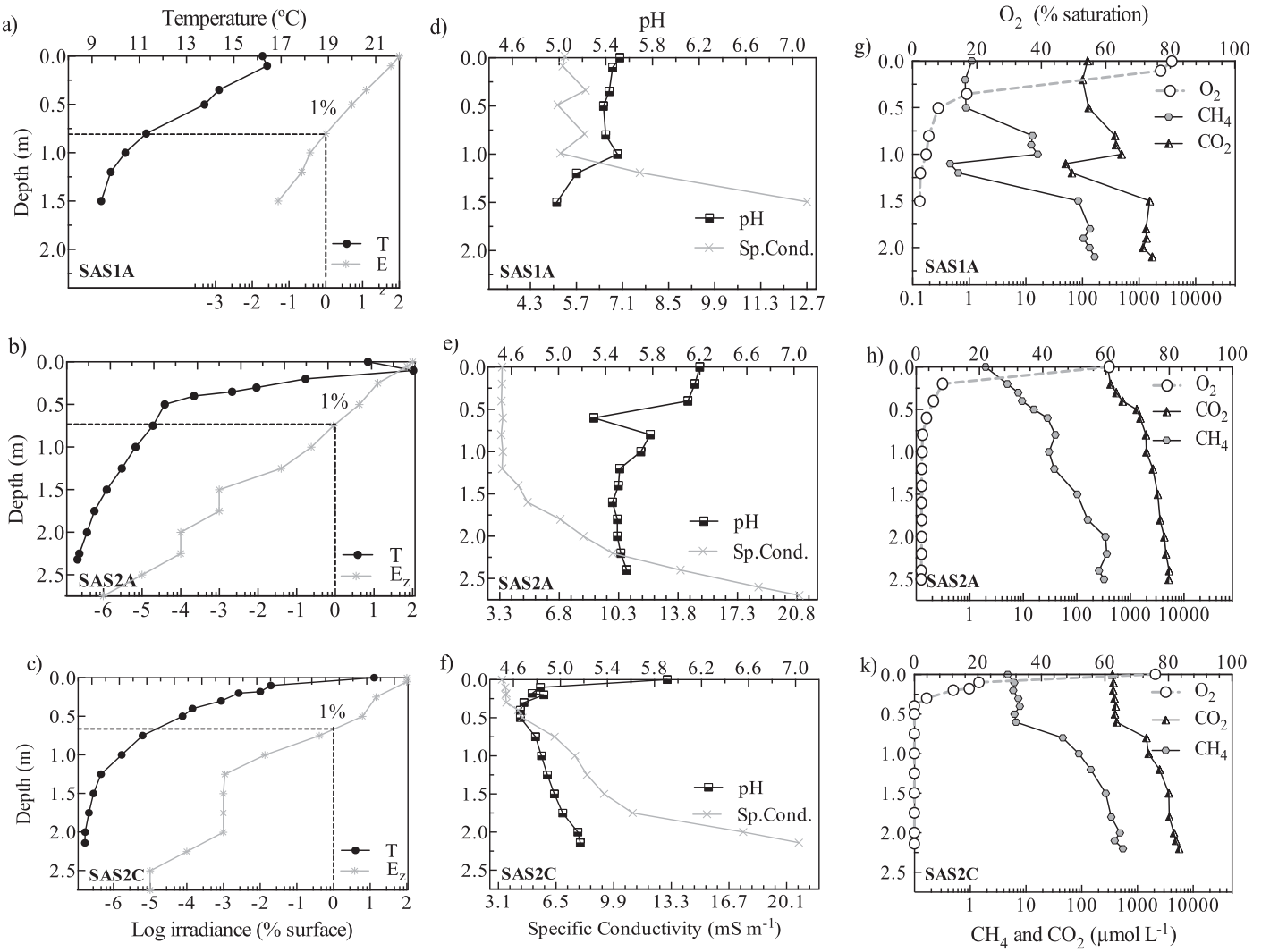

Fig. 5. Limnological profiles in southern palsa lakes SAS1A (top three panels), SAS2A (middle row) and SAS2C (lower three panels). Panels **(a)**, **(b),** and **(c)** show vertical profiles of irradiance E_z (as % of the surface value) and water temperature T (°C), panels **(d)**, **(e)**, and **(f)** show the changes in pH and specific conductivity (Sp.Cond.) down the water column, and panels **(g)**, **(h)**, and **(k)** present vertical profiles of gas concentrations: dissolved oxygen (as % saturation), CH_4 and CO_2 in μmol L^{-1}.

fluxes were higher by 1–3 (CH_4) and 3–6 (CO_2) orders of magnitude, in striking contrast to thermokarst lakes studied elsewhere (Table 3). The molar ratios of CH_4 to CO_2 fluxes were highly variable among sites, including within the same lake and valley. For the SAS lakes, the diffusive flux ratios averaged 0.010 ($\pm$ 0.007, $n = 50$), while the ebullition flux ratio averaged 1.40×10^6 ($\pm$ 1.97×10^6, $n = 24$); for the BON lakes, these values were 0.013 ($\pm$ 0.005, $n = 14$) and 0.80×10^6 ($\pm$ 0.71×10^6, $n = 11$).

There was a consistent spatial pattern in the gas fluxes, with greater emissions of both CH_4 and CO_2 measured at the deeper, middle part of the lake, and lower values inshore, near the edge of the lake. This is seen in the overall data set of all sampled lakes, where there was a strong relationship between the gas partial pressures at the lake surface and the depth of the water column underneath: surface concentrations of both gases increased as a linear function of water column depth (Fig. 6; for CO_2 vs. lake depth, $R^2 = 0.32$, df = 38, $p = 0.013$; for CH_4 vs. lake depth, $R^2 = 0.41$, df = 38, $p < 0.0001$). This relationship was stronger when the depths for each sample were normalized to the maximum depth of the lake (data not shown): for CO_2 vs. relative lake depth, $R^2 = 0.44$, df = 39, $p = 0.004$; for CH_4 vs. lake depth, $R^2 = 0.71$, df = 39, $p < 0.0001$). There was no correlation between mid-lake diffusive fluxes and lake area; for the seven lakes in Supporting Information Table S1, CH_4 flux vs. area, $r = -0.37$, df = 5, $p = 0.41$; CO_2 flux vs. area, $r = -0.62$, df = 5, $p = 0.14$.

Table 1. Limnological characteristics at the surface and bottom of palsa lakes in the region of study, including dissolved organic carbon (DOC), total nitrogen (TN), total phosphorus (TP), planktonic chlorophyll *a* (Chl *a*), and aqueous concentrations of methane (CH_4) and carbon dioxide (CO_2).

Location	Lake	DOC (mg C L^{-1})	TN (mg N L^1)	TP (mg P L^{-1})	Chl-a (μg L^{-1})	CH_4 (μmol L^{-1})	CO_2 (μmol L^{-1})
Surface							
BON	B1A	9.4	0.302	0.013	0.35	0.8	72
	B1B	8.2	0.541	0.020	4.57	1.8	113
	B2A	6.6	0.524	0.047	2.58	0.3	51
	B3A	8.8	0.230	0.012	0.72	0.9	19
SAS	S1A	10.4	0.580	0.014	3.31	2.5	319
	S1B	14.7	0.702	0.003	3.44	4.0	483
	S2A	8.5	0.420	0.015	0.94	5.0	799
	S2B	12.8	0.611	0.015	1.54	3.6	351
	S2C	11.0	0.591	0.017	2.24	6.2	583
Bottom							
BON	B1A	8.8	0.301	0.013	0.72	8.9	69
	B1B	8.2	0.538	0.026	-	1.9	109
	B2A	7.0	0.523	0.047	-	14.7	206
SAS	S1A	13.4	1.760	0.054	4.13	165	1712
	S1B	14.6	0.890	0.030	6.22	-	-
	S2A	9.0	0.404	0.016	3.34	273	5412
	S2B	22.0	1.881	0.057	7.78	292	3872
	S2C	21.0	1.710	0.044	1.84	552	5613

Table 2. Surface and bottom water concentrations of CO_2 and CH_4 in northern (BON) and southern (SAS) peatland thermokarst lakes. Each value is the mean of 17 (BON surface), 17 (BON bottom), 41 (SAS surface) and 35 (SAS bottom) samples (± SD) taken during mid-late summer 2012–2014. All values are well above the air-equilibrium concentrations for CH_4 and CO_2 (ca. 0.003 μmol CH_4 L^{-1} and 20 μmol CO_2 L^{-1}).

		Gas concentration (μmol L^{-1})	
Gas	Depth	BON	SAS
CH_4	Surface	0.88(0.64)	6(5)
	Bottom	2.20(1.72)	285(174)
CO_2	Surface	69(24)	359(131)
	Bottom	209(52)	2434(1852)

Sources of variation

Our estimates of CO_2 and CH_4 concentrations and fluxes are subject to multiple sources of variation, including analytical error, temporal variability, spatial variability (within and among lakes), and errors associated with model calculations. As an estimate of analytical and manipulation error, we examined the coefficients of variation (CV) for duplicate samples taken on 5 dates from the mid-lake surface waters of SAS2A. For CO_2, the CVs averaged 6.2% (range = 1.6–13.1%) and for CH_4 they averaged 9.7% (range = 2.1–23.1%). These variations are small relative to the observed inshore-offshore gradients (> 50%; Fig. 6) in gas concentrations.

As an indication of the potential error introduced in sampling at different periods of the day, a further measure of variability is provided by the measurements of gas concentrations in the near surface waters of SAS2A over 24 h, with duplicate samples for headspace determinations taken every 6 h from 18:00 h August 2 to 12:00 h August 3, 2013. The diurnal variation in CO_2 concentrations was small, with an average value for the four sampling times of 405 μmol L^{-1} (CV = 11%). An ANOVA analysis of all data (duplicate measurements at each of four times) showed a significant effect of time ($F_{3,4} = 20.0$, $p = 0.007$); subsequent Holm-Sidak pairwise tests showed that only the 0:00 value was significantly different from those at 12:00 h, 18:00 h, and 24:00 h ($t = 6.2$, 7.0, and 5.4, respectively; df = 2, $p \leq 0.022$), and was 16% above the overall mean. The near-surface CH_4 concentrations showed a greater degree of variability among sample times, with a mean of 2.74 μmol L^{-1} (CV = 25%). The ANOVA analysis for all the CH_4 data also showed a significant effect of time ($F_{3,4} = 9.2$, $p = 0.029$). The subsequent pair-wise tests showed only one significant difference: the 18:00 h sampling was significantly below that at 24:00 h ($t = 5.0$, df = 2, $p = 0.045$), and was 25% below the overall mean.

As measure of variability associated with model parameter estimations, we calculated the effects of a 20% error on gas concentrations and wind speed for estimates of diffusive CH_4 fluxes using Eq. 1. For an increase in CH_4 concentration from 3.60 μmol L^{-1} to 4.32 μmol L^{-1}, the estimated CH_4

Table 3. Diffusive and ebullition fluxes of CH_4 and CO_2 in sampled thermokarst lakes presented in comparison to results from four other permafrost regions. Palsa, thermokarst lake in palsa peatlands; Therm., thermokarst lake.

Location*	Lake and permafrost type*	Lat. deg N	Diffusive flux (mmol m^{-2} d^{-1})		Ebullition flux (mmol m^{-2} d^{-1})		Ref.†
			CH_4	CO_2	CH_4	CO_2	
SAS1	Palsa, S	55.1	1.0–12.8	4–55	<0.1–0.8	<0.001	[1]
SAS2	Palsa, S	55.1	1–10	40–242	0.01–0.5	<0.001–0.1	[1]
BON1	Palsa, E	57.5	0.1–0.9	20–58	<0.01–0.03	<0.001	[1]
BON2	Palsa, E	57.5	0.01–0.5	15–32	<0.01–0.02	<0.001	[1]
Finland	Boreal, I	61.5	0.2–0.8	9–25	0.2–13	0.002–0.05	[2]
Siberia	Therm., C	>45	0.07–0.22	-	2.1	-	[3]
Alaska	Therm., C	68.6	0.2	12–59	0–1558§	0–450	[3, 4]
Canada	Therm., C	73.0	0.002–6.3	(−8)−76.9	0.01–2.13	0.002–0.092	[5]

*See Fig. 1 for definition of the permafrost abbreviations;
†[1] This study; [2] Huttunen et al. 2006; [3] Walter Anthony et al. 2010; [4] King 1992; [5] I. Laurion, unpubl. data;
§Annual average extrapolated from point source data in [3].

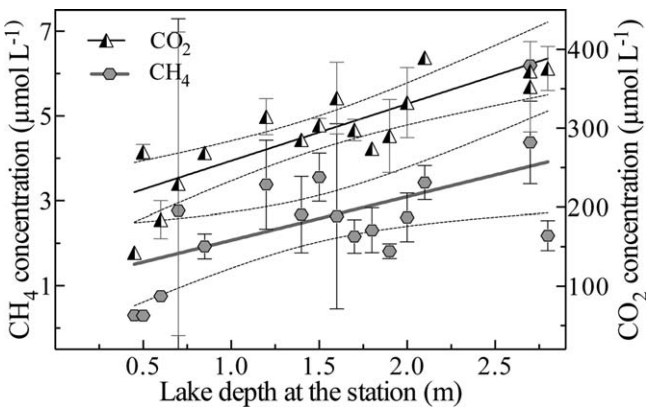

Fig. 6. Dissolved gas concentrations at the lake surface across all SAS sites as a function of water column depth directly beneath the position of sampling.

flux would increase by 21% from 4.8 mmol m^{-2} d^{-1} to 5.8 mmol m^{-2} d^{-1}. Changes in wind speed have a slightly greater effect: for a 20% increase from 3.37 m s^{-1} to 4.04 m s^{-1}, the estimated CH_4 flux would increase by 25% from 4.8 mmol m^{-2} d^{-1} to 6.0 mmol m^{-2} d^{-1}.

Radiocarbon dates

Gas concentrations in the bubbles were highly variable, and the two gases differed markedly in their radiocarbon ages, with the CH_4 containing much older carbon (Table 4). There were also large differences between SAS and BON. The $\Delta^{14}C$ values ranged from 83 to −277 ppt for CH_4 and from 24 to −517 ppt for CO_2, which corresponded to ages up to 2005 yr before present (BP) for CH_4 and 415 yr BP for CO_2 in the southernmost sites, and up to 760 yr BP for CH_4 and 120 yr BP for CO_2 in the northernmost sites (Table 4).

Table 4. Average water CH_4 and CO_2 concentrations in the hypolimnion (considered a storage flux source), and in the gas emitted via ebullition, with ^{14}C ages in yr BP (SD of ± 15–20 yr for all dates). The samples were obtained from the 2012–2014 campaigns. SD = standard deviation; *n* = number of observations.

Gas	Lake	Lakewater			Bubbles			
		μmol L^{-1}	SD	*n*	μmol L^{-1}	SD	*n*	^{14}C age
CH_4	SAS1A	669	221	22	11002	310	5	2005
	SAS1B	-	-	-	12842	298	3	-
	SAS2A	165	139	12	6367	6537	5	1360
	SAS2B	159	127	8	91	127	4	-
	SAS2C	364	147	6	7631	2014	7	-
	BON1A	2.4	3.1	7	5633	6221	5	760
	BON1B	1.7	0.9	4	4.5	0	2	-
CO_2	SAS1A	17500	1715	22	155	110	6	415
	SAS1B	-	-	-	712	39	3	-
	SAS2A	3427	1533	12	760	484	5	Modern
	SAS2B	2964	719	8	397	299	4	-
	SAS2C	4165	1093	6	674	622	7	-
	BON1A	707	88	7	133	88	5	120
	BON1B	210	5.9	4	872	0	2	-

Dating of surficial lake sediments at SAS1B gave values of 2735 yr BP for the top 3 cm of flocculent material, 2775 yr BP for the layer 3 cm to 6 cm, 3000 yr BP for the layer 6 cm to 10 cm, and 3285 yr BP for the bottom layer of the sediment core, from 10 cm to 12 cm.

Discussion

Palsa landscapes are common throughout the discontinuous permafrost zone, and descriptions of their geomorphology

often include mention or photographic evidence of their associated thermokarst lakes; for example, in eastern Canada (Kuhry 2008), western Canada (Turner et al. 2014), western Siberia (Pokrovsky et al. 2014), northern Sweden (Christensen et al. 2012), Iceland (Saemundsson et al. 2012), and interior Alaska (Kanevskiy et al. 2014). However, despite the circumpolar abundance of such lakes, their limnology has been little explored. The results of the present study show that palsa-associated thermokarst lakes in two contrasting regions of permafrost degradation shared a number of distinctive limnological characteristics, including high DOC, darkly colored waters, small surface areas, shallow depths, and strong physical and chemical gradients down their water columns. Concentrations of CO_2 and especially CH_4 were well above air-equilibrium values in the surface waters of all of these lakes, and both gases increased in concentration by orders of magnitude with depth, generally in tandem with a drop in oxygen tensions to hypoxic or anoxic conditions near the bottom sediments.

The highly stratified nature of certain types of thermokarst lakes has been attributed to their short wind fetch for mixing, the strong near-surface absorption of solar radiation, and the accumulation of solutes in the bottom waters due to mineralization processes in the sediments and freeze-concentration effects during winter (Deshpande et al. 2015). Palsa-associated thermokarst lakes represent an extreme set of conditions for these effects, with wind fetches of the order of tens of m or less, and the attenuation of solar irradiance to 1% of surface values within the upper 2 m of the water column (Figs. 4, 5). Additionally, the lakes are partially sheltered from winds coming from the direction of their associated palsas (Fig. 2), which may be 10 or more m wide and several m in height, thereby dampening the extent of wind-induced mixing. The resultant stratification combined with strong respiratory demand for oxygen in these DOC-rich waters would favor the loss of oxygen near the sediments, and anoxic conditions that are conducive to planktonic as well as benthic methanogenesis.

The diffusive fluxes for both gases were at or above the high end of ranges reported for lakes elsewhere, including other types of thermokarst waters (Table 1). This was particularly striking for the CH_4 fluxes, which had maximum values at and above 10 mmol m^{-2} d^{-1}, compared with < 1 mmol m^{-2} d^{-1} in other types of thermokarst lakes and ponds. In a comparison of lakes in the Canadian boreal zone, south of the present study, diffusive fluxes for CH_4 averaged around 1 mmol m^{-2} d^{-1}, but maximum values extended up to 20 mmol m^{-2} d^{-1} in some lakes (Rasilo et al. 2015). In that study, the CH_4 fluxes increased with decreasing lake area, which the authors attributed to shallower water columns, the increased tendency towards bottom anoxia and the higher ratio of sediments to water volume, which are all also features of the small thermokarst lakes sampled in the present study.

Although the diffusive CH_4 fluxes measured in the present study are large relative to other types of thermokarst lakes, they are not unusually high relative to peatland lakes and ponds further to the south. In a recent set of global estimates for northern waters, Wik et al. (2016) report that peatland lakes (outside the permafrost zone) have diffusive fluxes that are on average 2.6 times those measured in thermokarst lakes, and their compiled diffusive rates for this peat-based class of waterbodies (mean of 5.4, range of 1.6 mmol CH_4 m^{-2} d^{-1} to 7.6 mmol CH_4 m^{-2} d^{-1}) overlap with our data from the SAS valley peatland thermokarst lakes: mean of 4.8, range of 1.4 mmol CH_4 m^{-2} d^{-1} to 22.5 mmol CH_4 m^{-2} d^{-1}. In part this may reflect the order of magnitude greater soil carbon concentrations found in peatlands, including permafrost peatlands, relative to yedoma soils. The small size of peatland water bodies in general is also likely to be a factor contributing to their high rates of methanogenesis and CH_4 emission. All of the lakes in the present study were below the remote-sensing cut-off of 0.002 km^2 in the analyses by Wik et al. (2016), and there is increasing attention to the importance of small ponds that can have exceptionally high rates of greenhouse gas emissions (Holgerson and Raymond 2016).

One factor that may contribute to greater CH_4 fluxes from smaller lakes is the close physical coupling between the central regions of the lake and the littoral zone (Rasilo et al. 2015), where fluxes can be much higher than offshore. These high littoral fluxes have been attributed to warmer sediment temperatures inshore and the effects of wave action on sediment resuspension (Hofmann et al. 2010, 2013). In thermokarst lakes, the erosion of the surrounding permafrost may also play a role. For example, in a series of Siberian and Alaskan thermokarst lakes, a major source of CH_4 was from point source ebullition fueled by carbon released from permafrost degradation at the lake margins; offshore sources of CH_4 were also substantial, and derived from older sediment strata (Walter et al. 2006). In the present study, however, ebullition fluxes of CH_4 and CO_2 were likely limited to background ebullition (sensu Walter et al. 2006), while the diffusive emissions increased with overall water column depth, and maximum emission occurred in the central, deepest waters of the lake (Fig. 6). Several features of palsa-associated thermokarst lakes may give rise to this reverse pattern. Firstly, the lakes typically have steep sides, and they lack extensive shallows that could differentially heat up to provide warmer, inshore habitats for methanogens. Secondly the short fetch of the lakes means that little wave production occurs, and wave-induced sediment stirring is likely to be minimal. Finally, the transfer of eroded permafrost soils to the deeper part of the lake by sediment focusing, and the low oxygen conditions at the bottom of this central region, would likely favor the most rapid rates of methanogenesis, resulting in bubble production and transfer of gases to the surface, ultimately the atmosphere.

The production of quasi-stable microbubbles in supersaturated water has been identified as a potentially important pathway of CH_4 transfer from lakes to the atmosphere (Prairie and del Giorgio 2013; McGinnis et al. 2014), and could operate in the studied palsa lakes, where CH_4 concentrations are orders of magnitude above air equilibrium. Such microbubbles would rise at minimal rates through the water column, and their transfer to the lake surface would be largely dependent on turbulent mixing. However, if the bubbles formed through nucleation in the highly supersaturated bottom waters and then continued to grow (Boudreau et al. 2001), they could eventually achieve sufficient flotation velocities that would allow them to float up into the surface waters. The shaking of water samples for head space analysis would extract the gas from such microbubbles (Prairie and del Giorgio 2013), contributing to the higher gas concentrations, hence diffusive flux estimates, over the deeper sites of the lakes.

Although ebullition is recognized to be a major mechanism for gas transfer from thermokarst lakes to the atmosphere (Walter et al. 2006), it is difficult to accurately quantify. Bubble production is highly variable in space and time, with bubble size being one of several important factors influencing this variability (DelSontro et al. 2015). The ebullition fluxes that we measured here were unexpectedly lower than the diffusive fluxes, by one or more orders of magnitude (Table 1). Our highest measured ebullition rate (0.8 mmol CH_4 m^{-2} d^{-1}) lies near the low end of the ebullition range for thermokarst lakes as compiled in Wik et al. (2016): 0.4–8.2 mmol CH_4 m^{-2} d^{-1}. The bubble CH_4 concentrations (Table 4) overlapped with other studies: in percentage terms, the mean CH_4 concentration in all our ebullition data was 16%, with a maximum up to 83%; this compares with the range of 4–107% (all lakes) and 34 to >80% (Arctic lakes) as compiled in Walter Anthony et al. (2010). However, the volumetric gas fluxes were low. The mean flux for all of our ebullition measurements was 0.046 L m^{-2} d^{-1}, with large site-to-site variability (range = 0.006 L m^{-2} d^{-1} to 0.118 L m^{-2} d^{-1}). The mean ebullition flux for thermokarst lakes reported in Wik et al. (2016) was 87.5 mg CH_4 m^{-2} d^{-1}, which for an average CH_4 concentration in the bubbles of 40% would convert to 0.306 L m^{-2} d^{-1}, more than a factor of 6 higher than in the present study. Our measurements covered a wide range of lakes and within-lake locations, and were made during the warmest time of year when CH_4 production and ebullition rates might be expected to be high. It is possible that our sampling funnels failed to capture sparsely distributed active point sources such as seeps and hotspots (Walter Anthony et al. 2010) within the lakes, although these were never observed despite many sampling visits, and are not apparent in automated camera images of the lakes during freeze-up (Pienitz et al. 2016). The traps were deployed for only a short period of time, and possibly missed important periods of bubble production. For these reasons, the ebullition fluxes (Table 3) could be substantially underestimated. It is also possible that palsa-associated thermokarst lakes, underlain by a continuous layer of organic-rich, ancient peat, have more homogeneous sediments than yedoma systems, and that ebullition is dominated by low background rates rather than by point sources.

The dominance by diffusive fluxes (which could also include microbubble fluxes; Prairie and del Giorgio 2013) was especially due to the markedly high concentrations of CH_4 and CO_2 in the surface waters. The high CH_4 concentrations are consistent with microbiological studies in these lakes, which show an unusually high percentage of aerobic methanotrophs among the bacterial RNA sequences (Crevecoeur et al. 2015). These organisms would be favored by the high CH_4 availability, however their activity along with that of anaerobic CH_4 oxidizers, appears to be insufficient to deplete the continuous supply of CH_4.

The present study was conducted during warm, open-water conditions over three summer periods, but other times of year may also be important for GHG production, or their release to the atmosphere. These lakes are covered by ice for more than 6 months of the year, and the liquid water remaining under the ice becomes anoxic soon after freeze-up (Deshpande et al. 2015). Such conditions would be favorable for ongoing methanogenesis over winter, leading to large accumulations of CH_4 as well as CO_2 that could be subsequently released to the atmosphere after ice-out, as found at more southern latitudes (e.g., Ducharme-Riel et al. 2015). However, heating and stratification occur in early spring in these waters, and it is not until convective mixing in fall that the water column is fully mixed (Deshpande et al. 2015); the winter as well as summer hypolimnetic accumulation may only then be fully vented as a storage flux to the atmosphere. Such emissions may occur as short but intense bursts that would be difficult to capture by punctual sampling visits (Ducharme-Riel et al. 2015). This release of stored gases (Table 4) is likely to be considerable relative to the daily fluxes; for example the integrated water column values at SAS2A (2.8 m) were 0.4 mol CH_4 m^{-2} and 8 mol CO_2 m^{-2}. Expressed as potential storage fluxes, these are equivalent to 40 d and 8 d, respectively, of the maximum measured diffusive fluxes from this lake.

The thermokarst lakes in the southern part (SAS) of the study region had orders of magnitude greater CH_4 and CO_2 concentrations compared to the northern sites (BON), and the calculated gas fluxes differed accordingly. Several features may contribute to these large differences, including the organic-rich permafrost deposits at the SAS site that are now degrading rapidly and collapsing into the lakes. Northern Québec has experienced rapid warming over the last few decades, and lakes in the SAS valley have become more numerous and larger (Bhiry et al. 2011; Fillion et al. 2014). As shown by the thermal profile data (Fig. 3), the SAS2A palsa still retains a permafrost core, but its temperature is only

slightly below freezing and it is vulnerable to further warming. The BON site also lies on thick peat deposits (Bhiry et al. 2007), however it remains within the northern discontinuous permafrost zone where we measured cooler air temperatures and a lesser number of thawing degree days. Ongoing warming could lead to the BON lakes following a trajectory towards SAS conditions, with lake expansion, permafrost carbon release into the waters and increased microbial activity leading to increased GHG emissions, amplified also by higher autochthonous production of organic matter under warmer catchment and lake conditions. Increased DOC concentrations would lead to the greater absorption of solar irradiance by surface waters, as observed in the SAS lakes, and this would exacerbate thermal stratification and anoxia. Climate warming is also likely to have a direct effect on microbial heterotrophs and CH_4 producers, especially given that methanogenesis has been observed to respond strongly to increased temperatures, across multiple scales, from microbial cells to ecosystems (Yvon-Durocher et al. 2014). However, if climate warming leads to colder hypolimnia and stronger water column stability persisting for longer periods each year, this effect could be slowed down.

The ^{14}C dating analysis was based on a limited number of samples, and will require further sampling and corroboration in the future. Nevertheless, results indicated a striking difference in radiocarbon age between CH_4 and CO_2 in the ebullition samples from the palsa lakes. This implies that in these thermokarst systems, CH_4 oxidation is not the primary source of CO_2, and that the emitted CO_2 and CH_4 are at least partly derived from separate carbon pathways, as reported for lakes in the Canadian High Arctic (Bouchard et al. 2015). The highly variable ratio of CH_4 to CO_2 fluxes ($CV \geq 40\%$) also indicates that these two processes are largely uncoupled, as does the difference in the timing of maximum concentrations during the diurnal sampling. At BON, and to a greater extent at SAS, the CH_4 was at least partially derived from old carbon, likely associated with materials that were only recently mobilized by permafrost thawing.

The differences in CH_4 dates between SAS and BON are consistent with differences in the extent of permafrost degradation at the two sites. In both regions, peat bogs developed soon after the marine recession, at around 5800 yr BP at SAS and 4000 yr BP at BON (Bhiry et al. 2011). At BON, three phases of palsa formation have been identified, at 3200 yr BP, 2000 yr BP, and 400 yr BP (Bhiry et al. 2007), while at the lower latitudes of SAS and the James Bay region, palsas did not form until towards the end of the Little Ice Age, around 200 yr BP (Tremblay et al. 2014). Palsa degradation likely started earlier in the warmer conditions at SAS relative to BON, and is currently progressing rapidly (Bhiry et al. 2011; Fillion et al. 2014), mobilizing older peat bog carbon. The oldest date for the CH_4 in SAS approaches that of the surficial sediments of SAS lakes (2735 yr BP), implying recent mobilization of ancient organic carbon delivered to the bottom of the lake. The younger age at BON is consistent with a lesser extent of thawing, and mobilisation of carbon in younger permafrost strata than at SAS. Dilution with carbon from modern sources such as macrophytes, phytoplankton and recent terrestrial vegetation will have reduced the average carbon age in the CH_4 samples. At both locations, the CO_2 carbon had a younger age, implying that more recent photosynthesis produced the carbon sources for aerobic bacterial heterotrophy in these waters, in contrast to the old carbon used in anaerobic methanogenesis.

In summary, our results show that peatland thermokarst lakes share a number of distinct limnological features including high DOC concentrations and strong emissions of CH_4 and CO_2. These freshwater ecosystems are widely distributed throughout discontinuous permafrost peatlands, and they differ from the yedoma class of thermokarst lakes, which lie in less organic soils. The measurements obtained in the present study are too limited in time and space to provide a robust estimate of the total greenhouse gas flux from all thermokarst lakes in northern permafrost peatlands, but given the vast area of this landscape type (1.4 million km^2; Tarnocai et al. 2009) and the high diffuse emission rates that we measured, there is a need to measure flux rates throughout the subarctic for this type of non-yedoma system. The much greater gas fluxes from SAS relative to BON waters implies that old permafrost carbon stocks will be increasingly thawed and converted to CH_4 in peatland thermokarst lakes as the southern limit of permafrost continues to move northwards with ongoing climate change.

References

Allard, M., and M. K.-Seguin. 1987. Le pergélisol au Québec nordique: bilan et perspectives. Géogr. Phys. Quat. **41**: 141–152. doi:10.7202/032671ar

Allard, M., D. Sarrazin, and E. L'Hérault. 2015. Borehole and near-surface ground temperatures in northeastern Canada, v. 1.3 (1988-2014). Nordicana **D8**. doi:10.5885/45291SL-34F28A9491014AFD

An, W., and M. Allard. 1995. A mathematical approach to modelling palsa formation: Insights on processes and growth conditions. Cold Reg. Sci. Technol. **23**: 231–244. doi:10.1016/0165-232X(94)00015-P

Arlen-Pouliot, Y., and N. Bhiry. 2005. Palaeoecology of a palsa and a filled thermokarst pond in a permafrost peatland, subarctic Québec, Canada. Holocene **15**: 408–419. doi:10.1016/0165-232X(94)00015-P

Bastien, J., A. Tremblay, and L. LeDrew. 2009. Greenhouse gas fluxes from Smallwood Reservoir and natural water bodies in Labrador, Newfoundland, Canada. Verh. Internat. Verein. Limnol. **30**: 858–861.

Bhiry, N., S. Payette, and É. C. Robert. 2007. Peatland development at the arctic tree line (Québec, Canada)

influenced by flooding and permafrost. Quat. Res. **67**: 426–437. doi:10.1016/j.yqres.2006.11.009

Bhiry, N., and others. 2011. Environmental change in the Great Whale River Region, Hudson Bay: Five decades of multidisciplinary research by Centre d'études nordiques (CEN). Ecoscience **18**: 182–203. doi:10.2980/18-3-3469

Bonilla, S., V. Villeneuve, and W. F. Vincent. 2005. Benthic and planktonic algal communities in a high Arctic lake: Pigment structure and contrasting responses to nutrient enrichment. J. Phycol. **41**: 1120–1130. doi: 10.1111/j.1529-8817.2005.00154.x

Bouchard, F., I. Laurion, V. Prieskienis, D. Fortier, X. Xu, and M. J. Whiticar. 2015. Modern to millennium-old greenhouse gases emitted from ponds and lakes of the Eastern Canadian Arctic (Bylot Island, Nunavut). Biogeosciences **12**: 7279–7298. doi:10.5194/bg-12-7279-2015

Boudreau, B. P., B. S. Gardiner, and B. D. Johnson. 2001. Rate of growth of isolated bubbles in sediments with a diagenetic source of methane. Limnol. Oceanogr. **46**: 616–622, 1578(erratum). doi:10.4319/lo.2001.46.3.0616, 10.4319/lo.2001.46.6.1578

Christensen, T., M. Jackowicz-Korczyn'ski, M. Aurela, P. Crill, M. Heliasz, M. Mastepanov, and T. Friborg. 2012. Monitoring the multi-year carbon balance of a subarctic palsa mire with micrometeorological techniques. Ambio **41**: 207–217. doi:10.1007/s13280-012-0302-5

Cole, J. J., and N. F. Caraco. 1998. Atmospheric exchange of carbon dioxide in a low- wind oligotrophic lake measured by the addition of SF6. Limnol. Oceanogr. **43**: 647–656. doi:10.4319/lo.1998.43.4.0647

Crevecoeur, S., W. F. Vincent, J. Comte, and C. Lovejoy. 2015. Bacterial community structure across environmental gradients in permafrost thaw ponds: Methanotroph-rich ecosystems. Front. Microbiol. **6**: 192. doi:10.3389/fmicb.2015.00192

Crusius, J., and R. Wanninkhof. 2003. Gas transfer velocities measured at low wind speed over a lake. Limnol. Oceanogr. **48**: 1010–1017. doi: 10.4319/lo.2003.48.3.1010

DelSontro, T., D. F. McGinnis, B. Wehrli, and I. Ostrovsky. 2015. Size does matter: Importance of large bubbles and small-scale hot spots for methane transport. Environ. Sci. Technol. **49**: 1268–1276. doi:10.1021/es5054286

Deshpande, B. N., S. Macintyre, A. Matveev, and W. F. Vincent. 2015. Oxygen dynamics in permafrost thaw lakes: Anaerobic bioreactors in the Canadian subarctic. Limnol. Oceanogr. **60**: 1656–1670. doi:10.1002/lno.10126

Ducharme-Riel, V., D. Vachon, P. A. del Giorgio, and Y. T. Prairie. 2015. The relative contribution of winter under-ice and summer hypolimnetic CO_2 accumulation to the annual CO_2 emissions from northern lakes. Ecosystems **18**: 547–559. doi:10.1007/s10021-015-9846-0

Fillion, M.-È., N. Bhiry, and M. Touazi. 2014. Differential development of two palsa fields in a peatland located near Whapmagoostui-Kuujjuarapik, Northern Québec, Canada. Arct. Antarc. Alp. Res. **46**: 40–54. doi:10.1657/1938-4246-46.1.40

Gao, X., C. A. Schlosser, A. Sokolov, K. Walter-Anthony, Q. Zhuang, and D. Kicklighter. 2013. Permafrost degradation and methane: low risk of biogeochemical climate-warming feedback. Environ. Res. Lett. **8**: 035014. doi: 10.1088/1748-9326/8/3/035014

Glew, J. R. 1991. Miniature gravity corer for recovering short sediment cores. J. Paleolimnol. **5**: 285–287. doi:10.1007/BF00200351

Golterman, H., and R. Clymo [eds.]. 1971. Methods for chemical analysis of fresh waters. IBP handbook No. 8., 3rd ed. for International Biological Programme. Blackwell.

Hesslein R. H., J. W. M. Rudd, C. Kelly, P. Ramlal, and K. A. Hallard. 1990. Carbon dioxide pressure in surface waters of Canadian lakes, p. 413–431. In S. C. Wilhelms and J. S. Gulliver [eds.], Air-water mass transfer. American Society of Civil Engineers.

Hofmann, H. 2013. Spatiotemporal distribution patterns of dissolved methane in lakes: how accurate are the current estimations of the diffusive flux path? Geophys. Res. Lett. **40**: 2779–2784. doi:10.1002/grl.50453

Hofmann, H., L. Federwisch, and F. Peeters. 2010. Wave-induced release of methane: Littoral zones as a source of methane in lakes. Limnol. Oceanogr. **55**: 1990–2000. doi: 10.4319/lo.2010.55.5.1990

Holgerson, M. A., and P. A. Raymond. 2016. Large contribution to inland water CO_2 and CH_4 emissions from very small ponds. Nat. Geosci. **9**: 222–226. doi:10.1038/ngeo2654

Hopkins, D. M. 1949. Thaw lakes and thaw sinks in the Imuruk Lake area, Seward Peninsula, Alaska. J. Geol. **57**: 119–131. doi:10.1086/625591

Huttunen, J. T., T. S. Vaïsänen, S. K. Hellsten, and P. J. Martikainen. 2006. Methane fluxes at the sediment–water interface in some boreal lakes and reservoirs. Boreal Environ. Res. **11**: 27–34.

Kanevskiy, M., T. Jorgenson, Y. Shur, J. A. O'Donnell, J. W. Harden, Q. Zhuang, and D. Fortier. 2014. Cryostratigraphy and permafrost evolution in the lacustrine lowlands of west-central Alaska. Permafr. Periglac. Proc. **25**: 14–34. doi:10.1002/ppp.1800

Karlsson, J., and others. 2010. Quantifying the relative importance of lake emissions in the carbon budget of a subarctic catchment. J. Geophys. Res. **115**: G03006. doi: 10.1029/2010JG001305

King, G. M. 1992. Ecological aspects of methane oxidation, a key determinant of global methane dynamics. Adv. Microb. Ecol. **12**: 431–468.

Kruger, J. P., J. Leifeld, and C. Alewell. 2014. Degradation changes stable carbon isotope depth profiles in palsa peatlands. Biogeosciences **11**: 3369–3380. doi:10.5194/bg-11-3369-2014

Kuhry, P. 2008. Palsa and peat plateau development in the Hudson Bay lowlands, Canada: Timing, pathways and causes. Boreas **37**: 316–327. doi:10.1111/j.1502-3885.2007.00022.x

Laurion, I., W. F. Vincent, S. MacIntyre, L. Retamal, C. Dupont, P. Francus, and R. Pienitz. 2010. Variability in greenhouse gas emissions from permafrost thaw ponds. Limnol. Oceanogr. **55**: 115–133. doi:10.4319/lo.2010.55.1.0115

Liebner, S., L. Ganzert, A. Kiss, S. Yang, D. Wagner, and M. M. Svenning. 2015. Shifts in methanogenic community composition and methane fluxes along the degradation of discontinuous permafrost. Front. Microbiol. **6**: 356. doi:10.3389/fmicb.2015.00356

Luoto, M., and M. Seppala. 2003. Thermokarst ponds as indicators of the former distribution of palsas in Finnish Lapland. Perm. Periglac. Proc. **14**: 19–27. doi:10.1002/ppp.441

MacDougall, A. H., C. A. Avis, and A. J. Weaver. 2012. Significant contribution to climate warming from the permafrost carbon feedback. Nat. Geosci. **5**: 719–721. doi:10.1038/ngeo1573

MacIntyre, S., A. Jonsson, M. Jansson, J. A. Damon, E. Turney, and S. D. Miller. 2010. Buoyancy flux, turbulence, and the gas transfer coefficient in a stratified lake. Geophys. Res. **37**: L24604. doi:10.1029/2010GL044164

McGinnis, D. F., and others. 2014. Enhancing surface methane fluxes from an oligotrophic lake: Exploring the microbubble hypothesis. Environ. Sci. Technol. **49**: 873–880. doi:10.1021/es503385d

Negandhi, K., I. Laurion, M. J. Whiticar, P. E. Galand, X. Xu, and C. Lovejoy. 2013. Small thaw ponds: an unaccounted source of methane in the Canadian High Arctic. PLoS One **8**: e78204. doi:10.1371/journal.pone.0078204

Pienitz, R., F. Bouchard, B. Narancic, W. F. Vincent, and D. Sarrazin. 2016. Seasonal ice cover and catchment changes at northern thermokarst ponds in Nunavik: Observations from automated time-lapse cameras, v. 1.0 (2014-2015). Nordicana **D24**. doi:10.5885/45418AD-AF6A8064C702444B

Pokrovsky, O. S., and others. 2014. Thermokarst lakes of Western Siberia: A complex biogeochemical multidisciplinary approach. Int. J. Environ. Stud. **71**: 733–748. doi:10.1080/00207233.2014.942535

Prairie, Y. T., and P. A. del Giorgio. 2013. A new pathway of freshwater methane emissions and the putative importance of microbubbles. Inland Waters **3**: 311–320. doi:10.5268/IW-3.3.542

Rasilo, T., Y. T. Prairie, and P. A. del Giorgio. 2015. Large-scale patterns in summer diffusive CH_4 fluxes across boreal lakes, and contribution to diffusive C emissions. Glob. Chang. Biol. **21**: 1124–1139. doi:10.1111/gcb.12741

Saemundsson, T., O. Arnalds, C. Kneisel, H. P. Jonsson, and A. Decaulne. 2012. The Orravatnsrustir palsa site in Central Iceland—Palsas in an aeolian sedimentation environment. Geomorphology **167–168**: 13–20. doi:10.1016/j.geomorph.2012.03.014

Schneider von Deimling, T., and others. 2015. Observation-based modelling of permafrost carbon fluxes with accounting for deep carbon deposits and thermokarst activity. Biogeosciences **12**: 3469–3488. doi:10.5194/bg-12-3469-2015

Schuur, E. A. G., and others. 2013. Expert assessment of vulnerability of permafrost carbon to climate change. **119**: 359–374. doi:10.1007/s10584-552 013-0730-7

Sepulveda-Jauregui, A., K. M. Walter Anthony, K. Martinez-Cruz, S. Greene, and F. Thalasso. 2015. Methane and carbon dioxide emissions from 40 lakes along a north–south latitudinal transect in Alaska. Biogeosciences **12**: 3197–3223. doi:10.5194/bg-12-3197-2015

Stainton, M., M. J. Capel, and A. Armstrong. 1977. The chemical analysis of freshwater. Can. Fish. Mar. Serv. Misc. Spec. Publ. **25**, 180 pp.

Stuiver, M., and H. A. Polach. 1977. Discussion: Reporting of ^{14}C data. Radiocarbon **19**: 355–363.

Tan, Z., Q. Zhuang, D. K. Henze, C. Frankenberg, E. Dlugokencky, C. Sweeney, and A. J. Turner. 2015. Mapping pan-Arctic methane emissions at high spatial resolution using an adjoint atmospheric transport and inversion method and process-based wetland and lake biogeochemical models. Atmos. Chem. Phys. Discuss. **15**: 32469–32518. doi:10.5194/acpd-15-32469-2015

Tarnocai, C., J. G. Canadell, E. A. G. Schuur, P. Kuhry, G. Mazhitova, and S. Zimov. 2009. Soil organic carbon pools in the northern circumpolar permafrost region. Global Biogeochem. Cycles **23**: 3327. doi:10.1029/2008GB003327

Tremblay, S., N. Bhiry, and M. Lavoie. 2014. Long-term dynamics of a palsa in the sporadic permafrost zone of northwestern Québec (Canada). Can. J. Earth Sci. **51**: 1–10. doi:10.1139/cjes-2013-0123

Turner, K. W., B. B. Wolfe, T. W. D. Edwards, T. C. Lantz, R. I. Hall, and G. Larocque. 2014. Controls on water balance of shallow thermokarst lakes and their relations with catchment characteristics: A multi- year, landscape-scale assessment based on water isotope tracers and remote sensing in Old Crow Flats, Yukon (Canada). Glob. Chang. Biol. **20**: 1585–1603. doi:10.1111/gcb.12465

Vachon, D., Y. T. Prairie, and J. J. Cole. 2010. The relationship between near-surface turbulence and gas transfer velocity in freshwater systems and its implications for floating chamber measurements of gas exchange. Limnol. Oceanogr. **55**: 1723–1732. doi:10.4319/lo.2010.55.4.1723

Vallée, S., and S. Payette. 2007. Collapse of permafrost mounds along a subarctic river over the last 100 years (northern Québec). Geomorphology **90**: 162–170. doi:10.1016/j.geomorph.2007.01.019

Vincent, W. F., I. Laurion, R. Pienitz, and K. M. Walter Anthony. 2013. Climate impacts on Arctic lake ecosystems, p.27–42. *In* C. R. Goldman, M. Kumagai, and R. D. Robarts [eds.], Climatic change and global warming of inland waters: Impacts and mitigation for ecosystems and societies. Wiley. doi:10.1002/9781118470596.ch2

Vonk, J. E., and others. 2015. Effects of permafrost thaw on arctic aquatic ecosystems. Biogeosciences **12**: 7129–7167. doi:10.5194/bg-12-7129-2015

Walter, K. M., S. A. Zimov, J. P. Chanton, D. Verbyla, and F. S. Chapin III. 2006. Methane bubbling from Siberian thaw lakes as a positive feedback to climate warming. Nature **443**: 71–75. doi:10.1038/nature05040

Walter Anthony, K. M., D. A. Vas, L. Brosius, F. S. Chapin III, S. A. Zimov, and Q. Zhuang. 2010. Estimating methane emissions from northern lakes using ice-bubble surveys. Limnol. Oceanogr.: Methods **8**: 592–609. doi:10.4319/lom.2010.8.0592

Wik, M., R. K. Varner, K. Walter Anthony, S. MacIntyre, and D. Bastviken. 2016. Climate-sensitive northern lakes and ponds are critical components of methane release. Nat. Geosci. **9**: 99–105. doi:10.1038/ngeo2578

Yvon-Durocher, G., D. Bastviken, R. Conrad, C. Gudasz, N. Thanh-Duc, A. St-Pierre, and P. A. del Giorgio. 2014. Methane fluxes show consistent temperature dependence across microbial to ecosystem scales. Nature **507**: 488–491. doi:10.1038/nature13164

Acknowledgments

The authors thank the Natural Sciences and Engineering Research Council of Canada (NSERC), the Network of Centres of Excellence project ArcticNet, the Canada Research Chair program, the Québec nature and technology research funds (FRQNT), the Centre for Northern Studies (CEN, Université Laval), the NSERC Discovery Frontiers project ADAPT (Arctic Development and Adaptation to Permafrost in Transition) and the Northern Science Training Program, for financial support to this study. We are grateful to Claude Tremblay for help at the field station, and Denis Sarrazin for valuable aid with field instruments, data acquisition and field sampling. We equally extend our gratitude to our colleagues Sophie Crevecoeur, Anna Przytulska-Bartosiewicz, Maciej Bartosiewicz, Paschale Bégin, and Jérôme Comte for their help, support and discussions; to Marie-Josée Martineau for laboratory assistance; and to the reviewers of this manuscript for their insightful comments and advice.

Submitted 4 September 2015
Revised 18 February 2016
Accepted 25 March 2016

Associate editor: Kimberly Wickland